Title
Concurrent Optimization of Cycle Length, Green Splits, and Offsets for the Diverging Diamond Interchange

Journal
Transportation Research Record Journal of the Transportation Research Board, 2676(12)

ISSN
0361-1981

Authors
Do, Dawson
Chen, Yen-Yu
Chang, Gang-Len

Publication Date
2022-12-01

DOI
10.1177/03611981221096664

Concurrent Optimization of Cycle Length, Green Splits, and Offsets for the Diverging Diamond Interchange

Dawson Do
Department of Civil and Environmental Engineering
University of California, Berkeley, CA 94720-1770
Email: daws@berkeley.edu

Yen-Yu Chen (Corresponding Author)
Assistant Professor
Department of Transportation & Logistics Management
National Yang Ming Chiao Tung University, Hsinchu City 300, Taiwan
Email: yychen804@gmail.com

Gang-Len Chang
Professor
Department of Civil and Environmental Engineering
University of Maryland, College Park, MD 20742
Email: gang@umd.edu

Submitted March 18, 2022

Dawson Do, Yen-Yu Chen, and Gang-Len Chang

ABSTRACT

Diverging diamond interchange (DDI) has received increased attention from the traffic community for its efficiency in reducing delays for on- and off-ramp vehicles. Due to the conflicting through movements between a DDI's two crossover intersections, its signal plan must concurrently consider the progression for all critical paths to ensure overall efficiency. In light of DDI's unique geometric features, the design of its signal plans typically starts with the cycle length and green splits for its two crossover intersections, and then employs available progression models to produce the optimal offsets for those critical paths. Such a two-stage design methodology, however, often cannot yield the system-wide optimal results, because the optimal progression bandwidth and signal settings are interdependent. Moreover, inefficient coordination between its two crossover intersections may cause excessive queues on the DDI's bridge segment. Hence, this paper presents a mixed-integer linear programming (MILP) model that can concurrently optimize the cycle length, green splits, and offsets for a DDI's two crossover intersections under the given traffic patterns and geometric constraints such as the link length. The results of extensive numerical analyses with a real-world DDI have confirmed the effectiveness of the proposed model and its robustness in response to demand fluctuation.

Keywords: Diverging Diamond Interchange; Signal Control; Concurrent Optimization; Signal Progression; Traffic Delay

INTRODUCTION

Diverging diamond interchange (DDI), as shown in **Figure 1**, has emerged as an increasingly popular design alternative for conventional diamond interchange, due to its efficiency for vehicles turning onto on-ramps and efficient navigation for through vehicles. The reduction in conflict points also makes DDI a safer and more efficient option for coordinating the freeway and arterial flows, especially in reducing angle and rear-end crashes, as well as crash severity (*1*). Furthermore, as reported in the literature, a properly designed DDI can reduce the delay by 60% and the number of stops by 50% (*2, 3*). Some researchers also concluded that DDI, compared with a conventional interchange, can better accommodate high traffic volume, most significantly for left-turn flows (*4, 5*).

Noticeably, the unique geometric features of DDI render it especially imperative to coordinate the signals at two crossover-intersections so as to ensure the progression of traffic flows, and to prevent overflows on the connection bridge and at the off-ramps. As such, concurrently optimizing cycle length, green splits, and offsets is essential for optimizing a DDI's efficiency. Hence, grounded in those well-established methodologies in signal control literature (e.g., *6, 7, 8, 9*), this study aims to provide a Mixed-Integer Linear Programming (MILP) model for concurrently optimizing a DDI's cycle length, green splits, and offsets that can achieve progression bandwidth maximization and delay minimization for critical path flows. Moreover, the proposed model is embedded with essential constraints to minimize the likelihood of off-ramp queue spillbacks and overflows on the connection bridge.

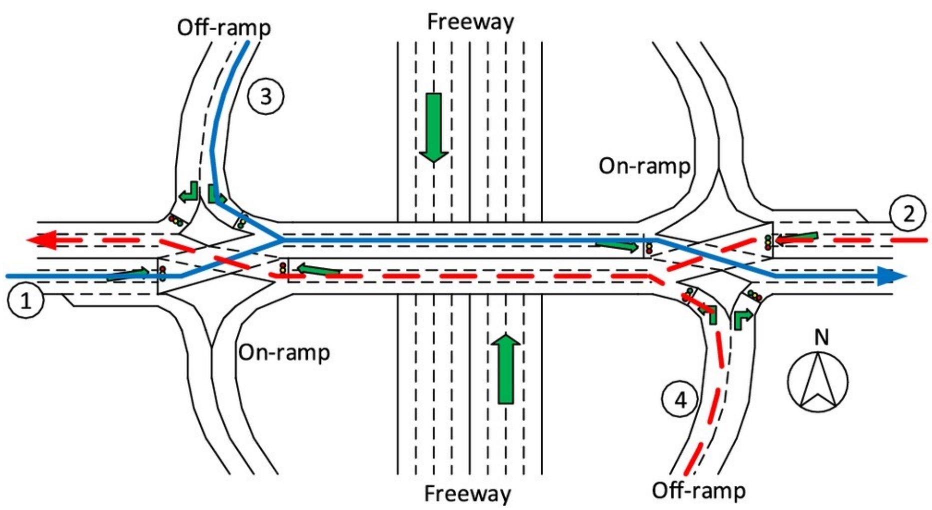

Figure 1 Geometric layout of a DDI and its critical paths

The rest of the paper is organized as follows. The next section provides a review of key studies related to DDI's signal control, followed by a detailed description of the proposed signal optimization model. Evaluation results along with the model sensitivity analyses constitute the core of the two ensuing sections. Concluding findings and future extensions are highlighted in the last section.

LITERATURE REVIEW

To promote DDI's implementation in practice, traffic researchers over the past decades have also devoted significant efforts to contending with various critical issues. Focusing on offset optimization for an existing corridor and DDIs, Day et al. (*10*) adopted high-resolution controller data and an enhanced link pivot algorithm to deconstruct the single-controller parameters into equivalent offset adjustments. They also (*10*) demonstrated the effectiveness of their proposed methodology over an arterial of five intersections, including a DDI, based on travel times collected with Bluetooth vehicle re-identification. In addition, Day et al. (*11*) investigated the effectiveness of three different strategies for cycle length for DDI coordination with six different origin-destination (O-D) scenarios through microscopic simulation. The strategies include (1) the full cycle length of the corridor; (2) a half-cycle; and (3) a three-phase scheme proposed by Hainen et al. (*12*) to manage the queues within a DDI. The measures of effectiveness (MOEs) were the number of stops, movement delays at the DDI, queue lengths, and delay by O-D path. The results show that utilizing half-length cycles at a DDI's crossover-intersections can reduce the delay for its movements. Moreover, Kim *et al.* (*13*) proposed a six-step procedure based on the dynamic bandwidth analysis tool (DBAT), developed for the North Carolina Department of Transportation (DOT) to allow for dynamic optimization of a signalized arterial, and to fine-tune the offsets of its DDI. Delay, stop severity index, maximum queue, and vehicle trajectory plots were adopted as the MOEs for evaluating their proposed approach.

In addition to the studies of optimizing a DDI's offsets, Yang *et al.* (*14*) developed a two-stage model to first produce the optimal cycle length and green times, and then the offsets for progression of the critical path flows between two crossover intersections. Cheng *et al.* (*15*) proposed a model for concurrent optimization of the crossover spacing and signal offsets to minimize the likelihood of incurring overflows on a DDI's bridge. Coogan and Thitsa (*16*) presented several data-driven traffic prediction models and control strategies for alleviating congestions at DDIs and their surroundings, and conducted evaluation with the field data from the DDI at the I-285 and Ashford Dunwoody Road and the DDI at the I-85 and SR 140/Jimmy Carter Boulevard. Concerning with such a design's effectiveness under real-time control, Kukić and Jovanović (*17*) presented a model with a fuzzy logic approach for an oversaturated DDI. Jovanović et al. (*18*) further included a ramp metering to their real-time control system to tackle the saturated or near saturated traffic condition on the freeway. In brief, most signal studies for DDI in the literature have not addressed the needs and benefits of concurrently optimizing the cycle length, offset, and green splits of a DDI.

Moreover, Yeom et al. (*19*) developed lane use models for DDI by revising the lane groups and predicting the upstream lane-use distribution with its downstream left-turn ratios. The field data collected from the Salt Lake City DDI were adopted for model validation. Most recently, the TRB National Cooperative Highway Research Program has produced a comprehensive guide for design of a DDI, including its essential geometric features, signal plan, safety concerns, and the need to accommodate multi-modal operations (*20, 21*).

MODEL FORMULATIONS

The core notion of the proposed model is to incorporate the progression logic of MAXBAND (*9*) in design of the cycle length and green splits of its crossover intersections. To ensure the maximal benefits of vehicles on all critical paths, this study has extended the design notion to maximizing the total weighted progression bandwidth and concurrently minimizing the total delay of vehicles in the queues. With the optimal interrelations between the cycle length, green splits, and progression bands, a DDI can thus best allocate its available capacity to critical traffic streams under different volume levels and traffic patterns.

Objective function for signal control

With the above-stated design notion, one shall specify its objective function as to maximize the sum of the progression bands, weighted with the volume on each path, and a penalty to account for the excessive delay experienced by the residual queues.

Equation 1 presents the objective function for the proposed DDI signal's concurrent optimization model, where K is the set of critical movements; J is the set of lane groups; φ is a weight factor for each movement or lane group; q is the hourly demand for each critical movement; b is the bandwidth (cycles); and V is the residual vehicles per hour in each lane group. The critical movements for the DDI are Eastbound Through (ET), Westbound Through (WT), Southbound Left (SL), and Northbound Left (NL), as shown in **Figure 1**. Note that the units for this objective function are vehicles per hour.

$$\text{Maximize: } \sum_{k \in K} \varphi_k q_k b_k - \sum_{j \in J} \varphi_j V_j \tag{1}$$

Constraints to ensure traffic progression

Figure 2 illustrates the relations between the progression bands and all signal-related variables as used in MAXBAND (*9*). The embedded interference constraints are shown in **Equation 2**.

$$0 \leq w_{ki} + b_k \leq \sum_m \alpha_{kmi} g_{mi} \, \forall k \in K, i \in I \tag{2}$$

where, w denotes the time period from the right (left) side of the red phase at intersection i to the left (right) boundary of the outbound (inbound) green band (cycles); g_{mi} is the green split of phase m at intersection i; and $\alpha_{kmi}=1$ if movement k receives a green time during phase m at intersection i and $\alpha_{kmi}=0$, otherwise. These formulations are designed for a two-phase signal plan, but the same methodology can be extended to signal controls with different phasing strategies such as the overlap control.

The second group of constraints is the loop integer constraints, similar to those formulated by Yang et al. (*14*). However, the crossover travel time, a decision variable, must be converted to the ratio of a cycle. As shown in **Figure 2** (a), such loop integer constraints for the left-turn paths can be expressed as follows:

$$(1 - g_{2E}) + w_{NL,E} + \frac{t_{NL} N}{3600} = \theta + (1 - g_{2W}) + w_{NL,W} + n_{NL} \tag{3}$$

$$w_{SL,E} + \frac{t_{SL} N}{3600} = -\theta + w_{SL,W} + n_{SL} \tag{4}$$

where, $t_{NL(SL)}$ is the crossover travel time for the northbound (southbound) left-turn (seconds); N is the number of cycles per hour; θ is the offset ratio, defined as the offset time duration over the cycle length, for the west intersection (cycle); and n_k is an integer variable for the number of cycles between the upstream and the downstream of the bandwidth for movement k, as shown in **Figure 2 (b)**. **Equations 3-6** formulate the relationship between the two intersections' signal plans using the offset and travel time. For example, in **Equation 3**, the total time duration between lines A and B in both intersections should be identical, as shown in **Figure 2 (a)**. The time duration from A to B at the east intersection is composed of $(1-g_{2E})$, $w_{NL,E}$, and $(\frac{t_{NL}N}{3600})$ (i.e., the left-hand side of **Equation 3**). Also, for the west intersection, the time duration from A to B includes, $(1-g_{2W})$, and $w_{NL,W}$. Thus, $((1-g_{2E})+w_{NL,E}+\frac{t_{NL}N}{3600})$ is equal to $(\theta+(1-g_{2W})+w_{NL,W})$. From these equations, the amount of bandwidth can be calculated using w.

By the same token, the through paths shall have the following similar constraints:

$$w_{WT,E}+\frac{t_{WT}N}{3600}=\theta+(1-g_{2W})+w_{WT,W}+n_{WT} \quad (5)$$

$$w_{ET,E}+\frac{t_{ET}N}{3600}=-\theta+(1-g_{1W})+w_{ET,W}+n_{ET} \quad (6)$$

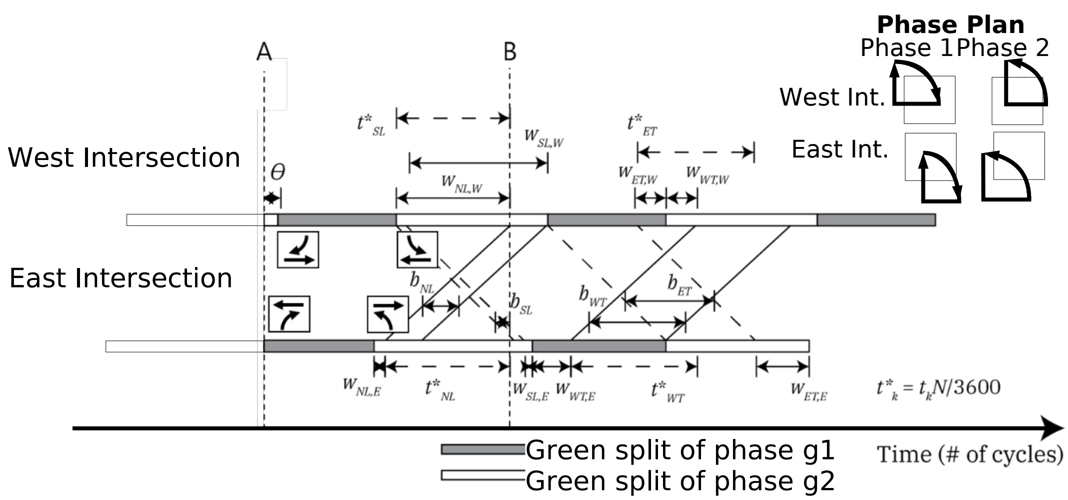

(a)

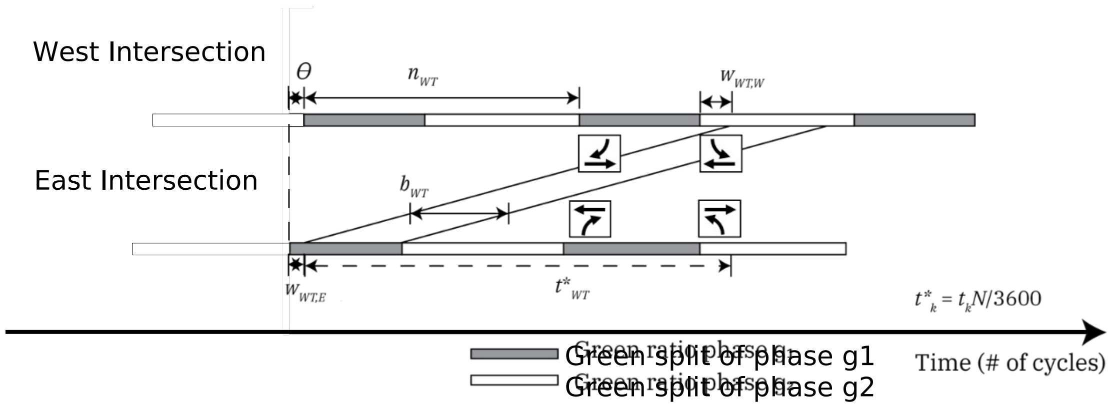

(b)

Figure 2 Graphical illustration of interrelations between progression and signal design variables (*14*)

Equations 7 and **8** represent the effective green bands that are required to begin after the downstream queues at the crossover intersection have been discharged, different from the conventional bandwidth that does not consider the discharging time of the downstream queues. Since the demands for all intersection approaches are given, one can then estimate the queue build-up and discharge times, as shown in **Equations 9** and **10**.

$$w_{NL,W} S \geq u_{WW}\left(q_{NL}\left(g_{2E}-b_{NL}\right)+q_{WT}\left(g_{1E}-b_{WT}\right)\right) \quad (7)$$

$$w_{WT,W} S \geq u_{WW}\left(q_{NL}\left(g_{2E}-b_{NL}\right)+q_{WT}\left(g_{1E}-b_{WT}\right)\right) \quad (8)$$

$$\left(g_{2E}-w_{SL,E}-b_{SL}\right) S \geq u_{EE}\left(q_{SL}\left(g_{2W}-b_{SL}\right)+q_{ET}\left(g_{1W}-b_{ET}\right)\right) \quad (9)$$

$$\left(g_{2E}-w_{ET,E}-b_{SL}\right) S \geq u_{EE}\left(q_{SL}\left(g_{2W}-b_{SL}\right)+q_{ET}\left(g_{1W}-b_{ET}\right)\right) \quad (10)$$

where, S is the saturation flow rate (veh/hr/ln); and $u_{WW(EE)}$ is the lane use factor for the westbound (eastbound) lane group at the west (east) intersection.

To ensure that the demand for each lane group is below the saturation level, one shall set the following additional constraint:

$$u_j Q_j \leq S\left(\sum_i \sum_m \beta_{mij} g_{mi} - N\zeta\right) + V_j \, \forall \, j \in J \quad (11)$$

where, Q is the hourly demand for the lane group, ζ is the loss time per cycle (hours); and $\beta_{mij}=1$ if lane group j is given the right of way during phase m at intersection i and $\beta_{mij}=0$, otherwise.

Additionally, **Equations 12** and **13** are set to prevent residual queues, vehicles which are not served over the first cycle, on the crossover bridge:

$$V_{EE}=0 \quad (12)$$

$$V_{WW}=0 \tag{13}$$

where, $V_{EE(WW)}$ is the residual queues per hour for the eastbound (westbound) lane group at the east (west) intersection.

Equation 14 is formulated to ensure that the maximal traffic queue under the optimal cycle will not exceed the available length of the turning bays.

$$\left(1-\sum_{i}\sum_{m}\beta_{mij}\,g_{mi}+N\zeta\right)u_j Q_j S \le l_j N\left(S-u_j Q_j\right)\forall j \in J \tag{14}$$

where, l_j is the storage space of the turning bay of lane group *j* (veh/ln).

Also, for each intersection i, its signal plan shall satisfy the following typical constraint:

$$\sum_{m} g_{mi}=1 \tag{15}$$

Lastly, for the offset,

$$0 \le \theta \le 1 \tag{16}$$

Optionally, one can also set the following constraints for the cycle length:

$$\frac{3600}{C_{\max}} \le N \le \frac{3600}{C_{\min}} \tag{17}$$

where, $C_{\max}$ and $C_{\min}$ are pre-defined maximal and minimal cycle lengths, respectively.

Noticeably, the entire model is a mixed-integer linear program and can thus be solved efficiently with existing methods in the optimization literature.

NUMERICAL ANALYSIS

The purpose of the experimental analysis presented hereafter is to verify the effectiveness of the proposed model in maximizing progression bandwidths. The geometric conditions and signal phases used for experimental investigation are based on the geometric features and initial signal plan for DDI in Manatee County, Florida, as illustrated in **Figure 3**. Other key parameters associated with the experiment site are summarized below:

- The lost time per cycle (for both phases) is given as 8 s
- The time for yellow and all-red phase is 10 s
- The saturation flow rate is 1,800 vehs/hr/lane
- The crossover free-flow travel time for the through and left-turn paths are 23 s and 16 s, respectively

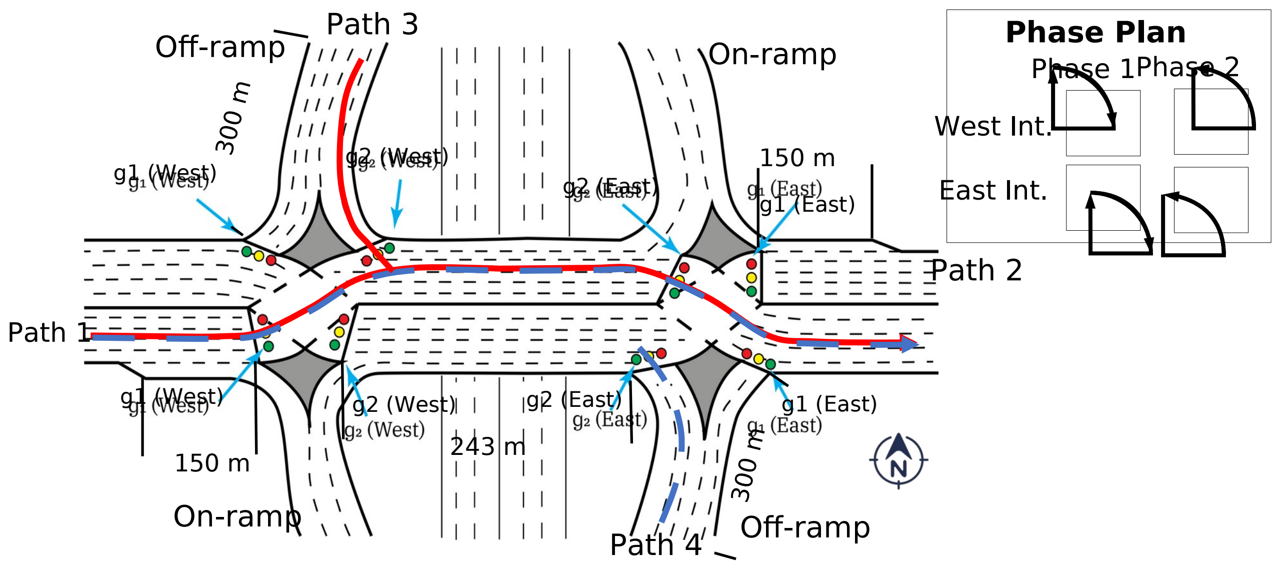

Figure 3 The geometric conditions, signal phases, and critical paths of DDI in Manatee County, Florida at the intersection of University Parkway and I-75

Table 1 shows all demand scenarios used for the performance evaluation, where:

- Cases 1 & 3: For testing the through-path dominant scenarios where most volumes are on the eastbound through and westbound through paths (i.e. paths 1 and 2 in **Figure 3**, respectively)
- Cases 2 & 4: For testing the left-turn dominant scenarios where a relatively large portion of the traffic comes from the off-ramps (i.e. southbound left-turn and northbound left-turn paths (see paths 3 and 4 in **Figure 3**, respectively)
- Case 5: For testing the scenario where one off-ramp left-turn path (southbound left-turn path, i.e. path 3) and one through path (westbound through path, i.e. path 2) experience relatively high volumes.

TABLE 1 Volume distributions for five experimental scenarios

unit: veh/hr

Case	Northbound		Southbound		Westbound			Eastbound			V/C ratio[1]
	L	R	L	R	L	T	R	L	T	R	
1	800	500	760	420	450	1600	450	510	1650	600	0.41
2	1200	500	1140	420	450	1200	450	510	1270	600	0.43
3	800	500	760	420	450	2200	450	510	2200	600	0.52
4	2000	500	1700	420	800	1500	750	900	1400	600	0.62
5	650	500	1300	420	450	1600	450	500	1000	600	0.45

[1] Estimated by FHWA CAP-X tool (*22*)

To evaluate the performance of the proposed concurrent model, this study has adopted *VISSIM* 10 (*23*) to estimate the measures of effectiveness (MOEs) under the five demand scenarios in **Table 1**. The proposed model was solved with *Xpress* (*24*) on a Windows 10 desktop. The MOEs, selected for performance comparison with the two-stage model from Yang (*14*) and Transyt-7F (*25*), are progression bandwidths, the average delay for each critical path, and the maximum queue length on the bridge. The latter two MOEs were taken from the average over ten simulation replications to account for the stochastic traffic nature embedded in the microscopic simulation. The entire simulation period is 1 hour with an additional 15-min of warm-up time. The parameters used in VISSIM have been calibrated with the field data collected from MD 295 and Arundel Mills Blvd. in Maryland with the GA algorithm based on the objective function shown below (i.e., **Equation 18**) (*14*). The resulting values of parameters are shown in **Table 2**.

$$min \frac{1}{N}\sum_{i=1}^{N} \text{¿¿¿} \qquad (18)$$

Where, Q_{bi} and Q_{si} are the observed and simulated maximum queue length at cycle i, respectively; and N is the number of cycles observed.

TABLE 2 The calibrated values for parameters used in VISSIM (*14*)

Parameters	Value
Desired speed distribution (car)	16.7 m/s (60 km/h)
Desired speed distribution (truck)	13.9 m/s (50 km/h)
Look ahead distance	0 ~ 304.8 m (0 ~ 1,000 ft)
Probability of temporary lack of attention	5%
Duration of temporary lack of attention	0.2 s
Average standstill distance	2.19 m (7.19 ft)

Note that without setting a reasonable upper bound, the proposed model may produce relatively long cycles, such as those of 208, 218, 188, and 208 s for cases 1, 2, 4, and 5, respectively (see **Table 3**). This is due to the embedded logic that the model intends to minimize the lost time by reducing the number of cycles while pushing the queue constraints. Hence, this study has adopted the upper bound of 150 s, as used in practice for the Manatee DDI, for the cycle length for all cases in the ensuing analysis. The key findings, based on the experimental results with respect to cycle length, green splits, and offsets are summarized below:

(1) Compared with the two-stage model and Transyt-7F, the bounded concurrent model yields the widest total progression bandwidth for all scenarios, except for Case 3, as shown in **Table 4**.

(2) Although the two-stage model yields a wider total bandwidth than the bounded concurrent model in Case 3, it has the highest weighted average delay among these models (i.e. 80.98 s/veh vs. 57.41 and 60.3 s/veh), as shown in **Figure 4 (c)**. The reason is that the proposed model maximizes the bandwidth with a penalty for the number of residual queue vehicles in its control objective function for concurrent design of the cycle length, phase settings, and offsets. But the two-stage and most existing models tend to first employ the capacity maximization to produce the optimal green splits, and then select the bandwidth maximization to design the optimal offsets. As such, the eastbound through path, having the highest volume among all approaches, with the two-stage model receives only 6.67% of the cycle length for its progression bandwidth (see **Table 4**).

(3) As shown in **Table 4**, Transyt-7F tends to give a wider bandwidth for eastbound and westbound through paths regardless of the demand distributions among critical paths. By contrast, the bandwidths by the concurrent model are more responsive to the volume distributions among critical paths in most cases. For example, in Case 4, where the northbound and southbound left-turn paths' demands are higher than all others, but Transyt-7F still gives these two through paths the widest bandwidth. By contrast, the concurrent model correctly assigns wider bandwidths to the NL and SL paths.

TABLE 3 Total signal splits and offsets under three candidate models

unit: second

Case	Model	East Crossover Signal			West Crossover Signal		
		Phase 1	Phase 2	Offset	Phase 1	Phase 2	Offset
1	Concurrent (Unbounded)	101	107	0	80	128	105
	Concurrent (Bounded)	61	89	0	63	87	64
	Two-stage	69	81	0	71	79	88
	Transyt-7F	70	80	0	72	78	75
2	Concurrent (Unbounded)	68	150	0	72	146	3
	Concurrent (Bounded)	53	97	0	56	94	7
	Two-stage	61	89	0	62	88	130
	Transyt-7F	53	97	0	61	89	75
3	Concurrent (Unbounded)	53	68	0	53	68	52
	Concurrent (Bounded)	53	68	0	53	68	52
	Two-stage	71	79	0	71	79	137
	Transyt-7F	72	78	0	72	78	75
4	Concurrent (Unbounded)	68	120	0	46	142	16
	Concurrent (Bounded)	61	89	0	42	108	16
	Two-stage	61	89	0	53	97	16
	Transyt-7F	62	88	0	55	95	75
5	Concurrent (Unbounded)	108	100	0	74	134	165
	Concurrent (Bounded)	47	101	0	51	97	132
	Two-stage	71	79	0	50	100	16
	Transyt-7F	72	77	0	50	99	76

TABLE 4 Resulting bandwidths under three candidate models

unit: % of the cycle length

Case	Critical Path	Bandwidth		
		Concurrent (bounded)	Two-Stage	Transyt-7F
1	ET	42.00	26.00	34.67
	WT	27.33	43.33	34.67
	SL	17.33	23.33	14.00
	NL	26.00	6.67	12.67
	Total	**112.66**	**99.33**	**96.01**
2	ET	22.00	2.67	34.67
	WT	8.67	28.00	34.67
	SL	47.33	56.67	25.33
	NL	58.67	35.33	24.00
	Total	**136.67**	**122.67**	**118.67**
3	ET	38.02	6.67	34.67
	WT	23.97	24.00	34.67
	SL	12.40	50.67	12.67
	NL	26.45	33.33	12.67
	Total	**100.84**	**114.67**	**94.68**
4	ET	16.00	20.67	34.67
	WT	14.67	10.00	34.67
	SL	61.33	43.33	22.00
	NL	68.67	59.33	24.00
	Total	**160.67**	**133.33**	**115.34**
5	ET	7.43	12.00	33.56
	WT	23.65	18.67	35.57
	SL	65.54	45.33	18.12
	NL	46.62	52.67	26.17
	Total	**143.24**	**128.67**	**113.42**

The average delay for each critical path in those five experimental cases under three candidate models is presented in **Figure 4**. Some key findings are summarized below:

(1) With respect to Case 1 that the through volumes are relatively higher than the turning ones, all three candidate models yield the same level of average delay for traffic flows over those four critical paths, ranging from the lowest of 55.94 s/veh for the proposed model to the highest of 57.91 s/veh for the Transyt-7F (see **Figure 4 (a)**). Notably, the proposed model tends to trade some delays in the through path flows (see path 2) to favor the left-turning off-ramp flows (i.e., path 4) so as to minimize the likelihood of spilling the off-ramp queues back onto the freeway mainline.

(2) For traffic scenarios of high left-turning volume (i.e., path 3 and path 4), as shown in Case 2, both the proposed model and the two-stage model are capable of allocating sufficient green durations to accommodate the off-ramp flows, and thus yield less delay than that with Transyt-7F on those target critical paths (see **Figure 4 (b)**). With respect to path 3, the resulting average delay with Transyt-7F is about twofold of that under the proposed model (66.36 sec/veh vs. 33.48 sec/veh). Moreover, the average delay with

Transyt-7F on path 4 is more than twofold of that with the proposed model (71.89 sec/veh vs. 31.70 sec/veh).

(3) Under the scenario of having dominated through volumes as shown in Case 3, the proposed model is more effective with respect to balancing the congestion level for all critical paths, and yields the more even distributions for their delays, compared with the other two models, among all critical path flows (see **Figure 4 (c)**). With such a desirable feature, the proposed model expectedly yields the lowest overall average delay (i.e., 57.41 s/veh) for all critical paths in such a highly congested traffic scenario.

(4) Under the traffic scenario of higher left-turning and through volumes, as shown in Case 4, all three models exhibit a comparable level of performance (i.e. 60.71, 61.64, and 67.14 s/veh for the concurrent model, two-stage model, and Transyt-7F, respectively), as shown in **Figure 4 (d)**. However, same as the results in Case 2, the proposed model tends to allocate its green times in favor of those left-turning off-ramp flows (i.e., path 3 and path 4). Such an allocation of green times is expected to mitigate the likelihood of having two off-ramp queues from the freeway to spill back onto its mainline.

(5) In Case 5 for testing the scenario of moderately high volumes at one off-ramp (i.e. path 3) and in one through traffic streams (i.e. path 2), the proposed model expectedly yields less average delay than with the other two models, especially for the heavy path 3 flows (i.e., 29.18 s/veh vs. 40.68 and 85.45 s/veh) that need to exercise left turns to exit the freeway. Aside from effectively responding to the needs of critical path flows, the proposed model's overall performance in this traffic scenario with respect to all four critical path flows is lower than those produced from the other two models, as shown in **Figure 4 (e)**.

In summary, the experimental results from five specially designed traffic scenarios seem to reflect the fact that the proposed model with its concurrent optimization of cycle length, green settings, and offsets can perform more effectively than the two well-established models with respect to accommodating the critical left-turn flows from the freeway off-ramps.

Note that ensuring smooth operations for such off-ramp flows is the most critical task for DDI. Conceivably, the proposed model with its embedded logic to favor the off-ramp left-turning flows under some traffic scenarios may render a higher average delay to those through traffic flows than that under those models based on the volume to allocate the green time (e.g., Tansyt-7F). However, the experimental results clearly show that the maximal traffic queue length on the connecting bridge of the DDI in all case studies will not exceed its length (see **Table 5**), and the overall performances with respect to all critical paths are slightly better than two established models (see **Figure 5**). Such a performance, however, may not be assured if with other models. For instance, in Case 3, if with the two-stage model, its queue length in the eastbound direction will be 246.1 meters, longer than the bay length of 243 meters.

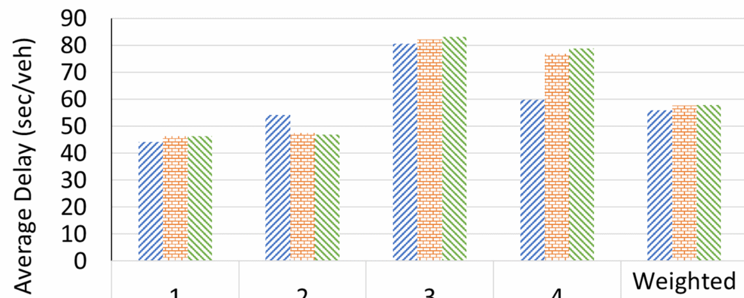

	1	2	3	4	Weighted Avg.
Concurrent Model (Bounded)	44.22	54.05	80.63	59.84	55.94
Two-Stage Model	46.31	47.57	82.08	76.92	57.63
Transyt-7F	46.34	46.87	83.16	78.76	57.91

unit: sec/veh

Critical Path

(a) Average Delays of Critical Paths - Case 1

	1	2	3	4	Weighted Avg.
Concurrent Model (Bounded)	72.43	87.48	33.48	31.70	56.76
Two-Stage Model	80.36	79.37	40.10	35.38	59.29
Transyt-7F	45.22	49.12	66.36	71.89	57.88

unit: sec/veh

Critical Path

(b) Average Delays of Critical Paths - Case 2

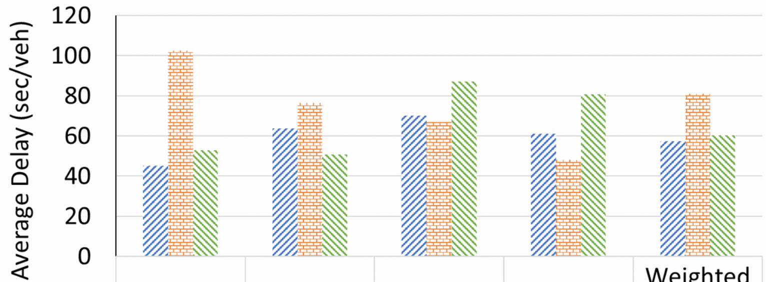

Critical Path	1	2	3	4	Weighted Avg.
Concurrent Model (Bounded)	45.21	63.71	70.23	60.98	57.41
Two-Stage Model	102.56	76.42	66.98	48.10	80.98
Transyt-7F	52.78	50.86	87.01	80.63	60.30

Critical Path

unit: sec/veh

(c) Average Delays of Critical Paths - Case 3

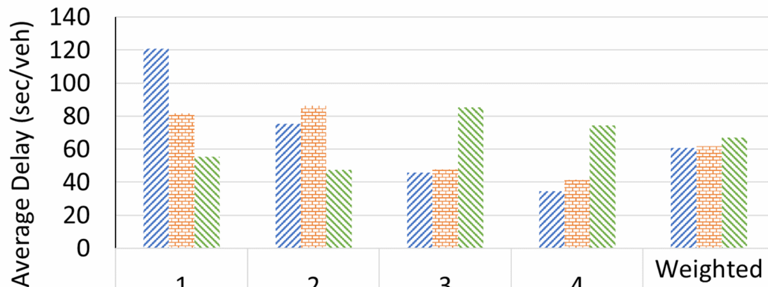

Critical Path	1	2	3	4	Weighted Avg.
Concurrent Model (Bounded)	120.69	75.30	45.66	34.59	60.71
Two-Stage Model	81.45	86.36	47.89	41.41	61.64
Transyt-7F	55.47	47.31	85.32	74.38	67.14

Critical Path

unit: sec/veh

(d) Average Delays of Critical Paths - Case 4

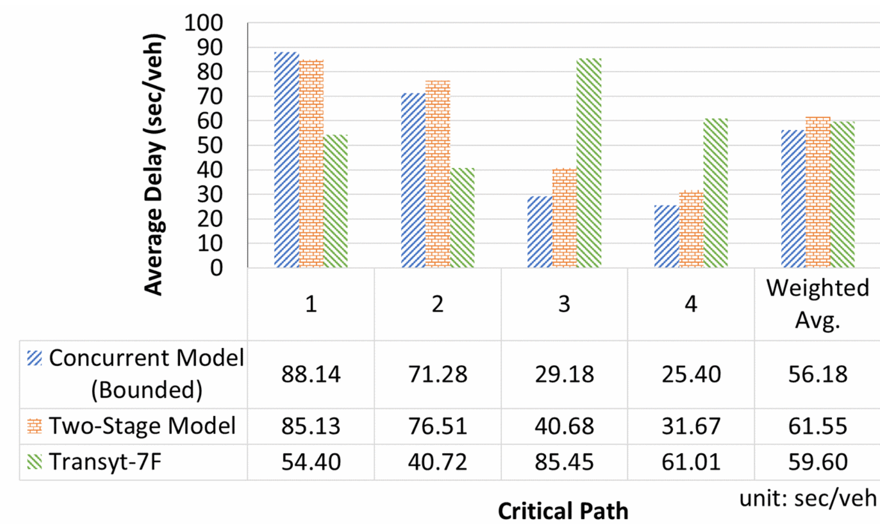

(e) Average Delays of Critical Paths - Case 5

Figure 4 Average delays of critical paths

TABLE 5 Queue lengths on the bridge

unit: meter

Case	Direction on the bridge	Queue Length		
		Concurrent (bounded)	Two-Stage	Tansyt-7F
1	Eastbound	70.7	80.7	80.6
	Westbound	66.4	72.4	72.4
2	Eastbound	99.9	98.7	81.3
	Westbound	122.4	92.1	80.4
3	Eastbound	74.1	246.1	96.0
	Westbound	121.4	227.9	87.8
4	Eastbound	222.8	220.1	139.5
	Westbound	107.7	235.9	162.5
5	Eastbound	107.4	120.7	107.9
	Westbound	139.8	144.8	66.4

Note: Bay lengths of both directions on the bridge are 243 meters.

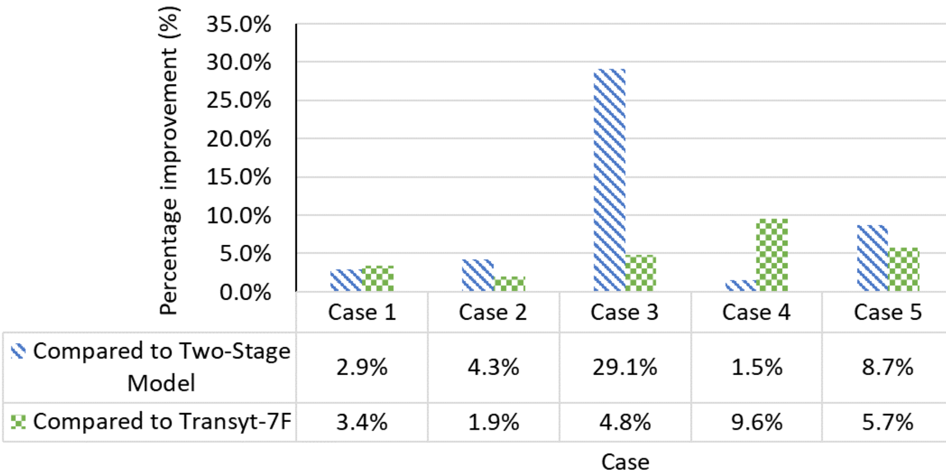

	Case 1	Case 2	Case 3	Case 4	Case 5
Compared to Two-Stage Model	2.9%	4.3%	29.1%	1.5%	8.7%
Compared to Transyt-7F	3.4%	1.9%	4.8%	9.6%	5.7%

Figure 5 Percentage improvements on weighted average delays

SENSITIVITY ANALYSIS

The robustness of this model in practice depends on its performance stability with respect to the temporal variation of field data and the responsiveness to demand surge. Therefore, based on the data in Case 1, this study has further analyzed the impacts of the following key inputs on the resulting control settings (i.e., cycle length, offset, and green splits):

- Crossover travel times
- Critical movement volumes

In conducting such sensitivity analyses, Case 1 was re-evaluated with the change of +5%, -5%, +20%, and -20% to each key input on those control parameters.

The results for Case 1, a traffic scenario dominated by the through volume, are shown in **Figure 6** and **Figure 7**, and also summarized below:

(1) The decision variables for the traffic scenario, including cycle length, offset, and green splits, are all stable with respect to variation in through and left-turn crossover travel times, as shown in **Figure 6 (a)** and **(b)**.

(2) When the ET path experiences a volume increase (decrease), the proposed model expectedly decreases (increases) the cycle length (see **Figure 6 (c)**) at those crossover signals so as to reduce the queues per cycle and the resulting delay, but accommodate the volume variation by concurrently adjusting the green splits and offsets. For instance, the green splits for the ET path flow, which are phase 1 at the west crossover signal and phase 2 at the east crossover signal, increase with the volume surge in the ET path flows. And the offset also reduces by 26% when the ET path demand increases by 20%, as shown in **Figure 6 (c)**. As the result, the bandwidth of the path increases by 4% (see **Figure 7**).

(3) Same as the volume surge in the ET path flows, the proposed model will also broaden the bandwidth of the WT path when encountering a significant increase in the WT path volume (see **Figure 7)** through adjusting those decision variables (see **Figure 6 (d)**).

(4) As for significant volume changes in the NL or SL path flows, the proposed model under this case of through-volume dominated scenarios tends to mainly adjust the

offsets for those two left-turning paths, and let the revised progression bands accommodate the new left-turn patterns. For example, even the volume in those two left-turn paths experiencing up to 20% fluctuation, the proposed model, as expected, will change only the offsets for those left-turn paths, but not the cycle length and green splits (see **Figure 6 (e)** and **(f)**) to accommodate the change in left-turn volume because the signal plan for both crossover intersections under this traffic scenario is determined primarily by the high through volumes.

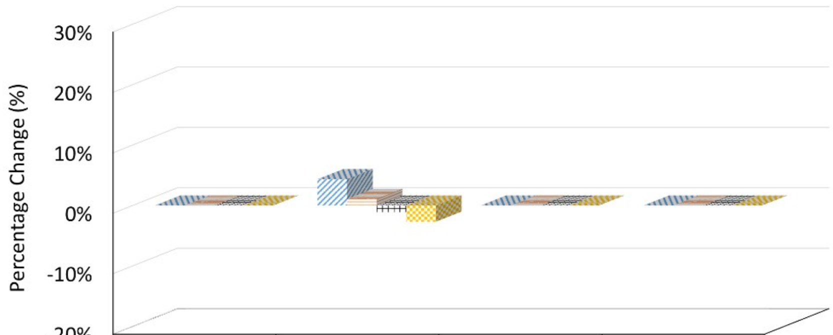

	Cycle Length	Offset	Green split of phase 1 (East signal)	Green split of phase 1 (West Signal)
Based travel time - 20%	0%	4%	0%	0%
Based travel time - 5%	0%	1%	0%	0%
Based travel time + 5%	0%	-1%	0%	0%
Based travel time + 20%	0%	-3%	0%	0%

Control Setting

(a) Through Travel Time vs. Decision Variables - Case 1 (Based Through Travel Time: 23 sec)

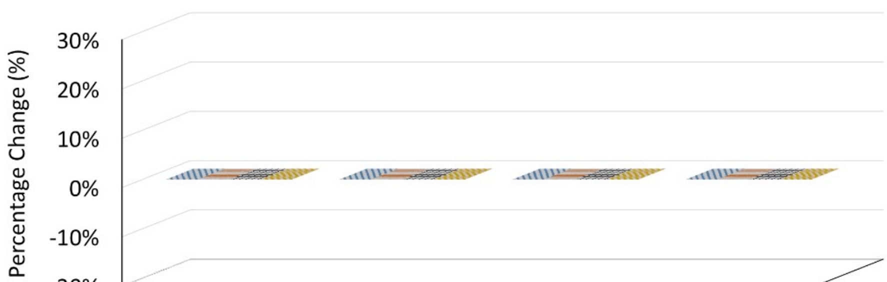

	Cycle Length	Offset	Green split of phase 1 (East signal)	Green split of phase 1 (West Signal)
Based travel time - 20%	0%	0%	0%	0%
Based travel time - 5%	0%	0%	0%	0%
Based travel time + 5%	0%	0%	0%	0%
Based travel time + 20%	0%	0%	0%	0%

Control Setting

(b) Left-turn Travel Time vs. Decision Variables - Case 1 (Based Left-turn Travel Time: 16 sec)

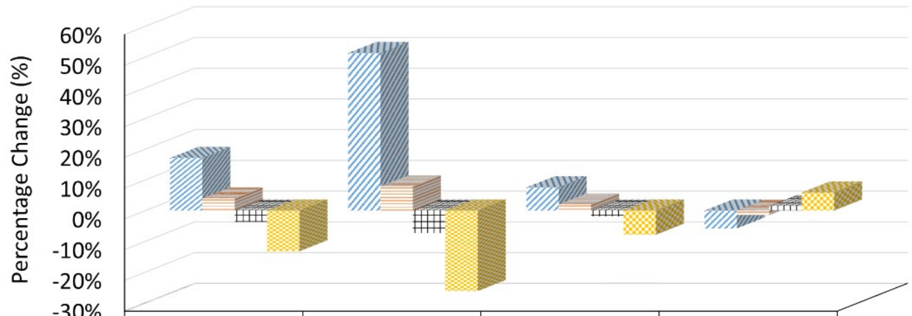

	Cycle Length	Offset	Green split of phase 1 (East signal)	Green split of phase 1 (West Signal)
Based demand - 20%	17%	51%	8%	-6%
Based demand - 5%	4%	8%	2%	-1%
Based demand + 5%	-4%	-7%	-2%	1%
Based demand + 20%	-13%	-26%	-8%	6%

Control Setting

(c) ET Path Demand vs. Decision Variables - Case 1 (Based ET Path Demand: 1,650 vph)

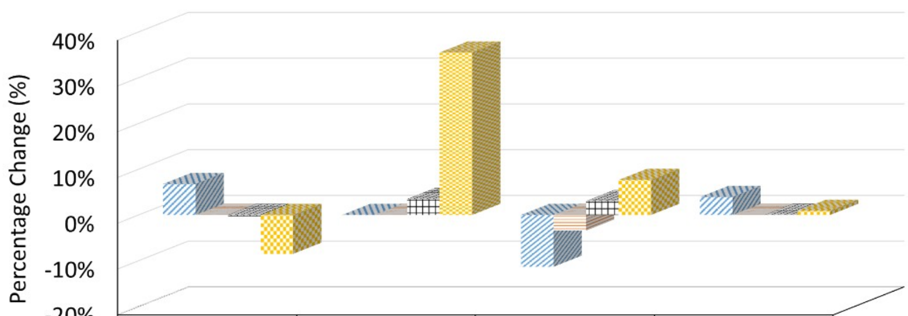

	Cycle Length	Offset	Green split of phase 1 (East signal)	Green split of phase 1 (West Signal)
Based demand - 20%	7%	0%	-11%	4%
Based demand - 5%	0%	0%	-3%	0%
Based demand + 5%	0%	3%	3%	0%
Based demand + 20%	-9%	35%	8%	1%

Control Setting

(d) WT Path Demand vs. Decision Variables - Case 1 (Based WT Path Demand: 1,600 vph)

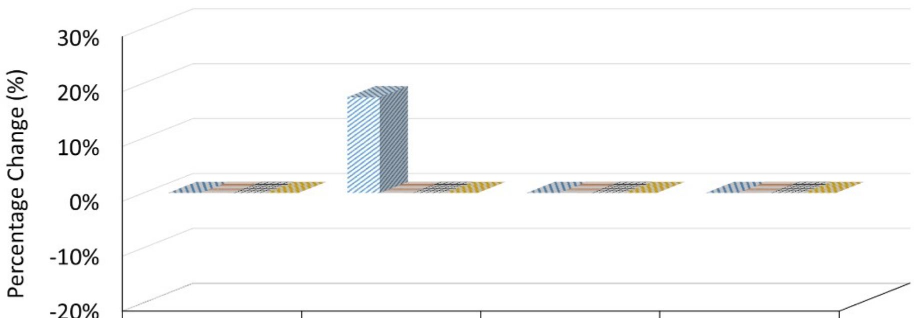

	Cycle Length	Offset	Green split of phase 1 (East signal)	Green split of phase 1 (West Signal)
Based demand - 20%	0%	17%	0%	0%
Based demand - 5%	0%	0%	0%	0%
Based demand + 5%	0%	0%	0%	0%
Based demand + 20%	0%	0%	0%	0%

Control Setting

(e) NL Path Demand vs. Decision Variables - Case 1 (Based NL Path Demand: 800 vph)

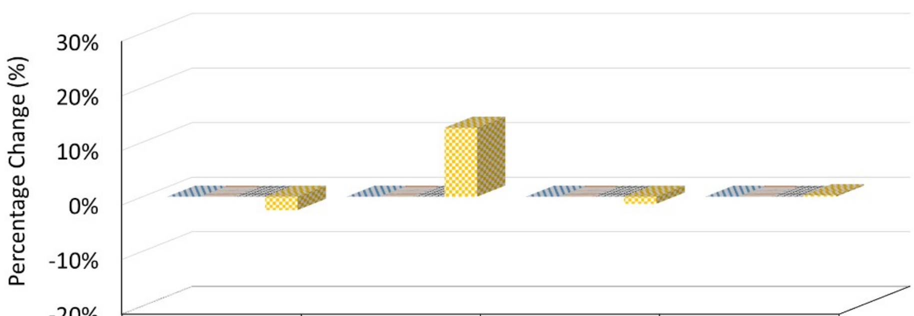

	Cycle Length	Offset	Green split of phase 1 (East signal)	Green split of phase 1 (West Signal)
Based demand - 20%	0%	0%	0%	0%
Based demand - 5%	0%	0%	0%	0%
Based demand + 5%	0%	0%	0%	0%
Based demand + 20%	-2%	13%	-1%	0%

Control Setting

(f) SL Path Demand vs. Decision Variables - Case 1 (Based SL Path Demand: 760 vph)

Figure 6 Relative changes in cycle length, offset, and green splits under different levels of volume changes

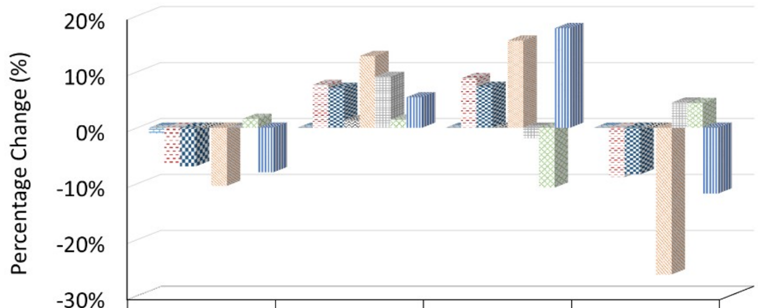

	NL	SL	WT	ET
Based NL Demand + 20%	-1%	0%	0%	0%
Based NL Demand - 20%	-7%	8%	9%	-9%
Based SL Demand + 20%	-7%	7%	7%	-8%
Based SL Demand - 20%	0%	1%	0%	0%
Based WT Demand + 20%	-10%	13%	16%	-26%
Based WT Demand - 20%	0%	9%	-2%	5%
Based ET Demand + 20%	2%	1%	-11%	4%
Based ET Demand - 20%	-8%	5%	18%	-12%

Critial Path

Figure 7 Relative changes in bandwidths under different volumes for Case 1

CONCLUSIONS

Due to the designated function and unique geometric features, a DDI's efficiency rests on its effective progression not only for vehicles over those two crossover intersections, but also for the freeway off-ramp traffic flows left-turning to the arterial. Hence, in design of a DDI's signal plan, one shall concurrently account for the coordination between its two crossover intersections, the formation of queues on the connection bridge and at the off-ramps. Intending to address this imperative issue, this study, grounded in the advancements in the traffic control literature, has presented an integrated control model that allows users to concurrently optimize cycle length, green splits, and offsets to maximize the progression for a DDI's path-flows and to minimize the likelihood of off-ramp queue spillback onto the freeway mainline or overflows on the connection bridge.

To evaluate the performance of the proposed concurrent DDI signal-control model, this study has designed several traffic scenarios based on a DDI in Florida where either its through arterial or left-turn off-ramp traffic exhibits as the predominant path flows. The experimental results evaluated with VISSIM have confirmed the expected performance of the proposed model, especially with respect to its unique strength in effectively responding to any path volume surge with concurrent adjustment of the cycle length and offsets. Most importantly, the proposed model's unique feature of allocating the green times and offsets to benefit the DDI's two off-ramp turning streams can constrain their flow rates to be within the available capacity, and thus prevent the formation of overflows over the connection bridge in most traffic scenarios. With respect to the system-wide average delay, the numerical analysis results have also revealed that the proposed model with its concurrent optimization features can produce better coordinated signal plans than with existing models for traffic scenarios of high through volumes or high left-turning and through volumes. In those typical traffic scenarios, the proposed model can yield the MOEs comparable to the state of practices. However, the proposed signal optimization model is for fixed-time signal design which may not be sufficiently responsive and effective for the scenarios exhibiting highly fluctuated flow patterns. A more robust optimization algorithm shall be considered in the future extension for its use in effective time-of-day controls. Also, to accommodate the practice of local traffic agencies and possibly the need of coordinating with neighboring conventional intersections, one may add an upper bound to the model's produced cycle length.

Some DDIs use a single controller for both crossover intersections. The methodology described above can be applied provided that the offset variable is removed and the green splits are set equal between both crossovers. A future extension of the proposed model will focus on including the connection bridge's length in the DDI's overall traffic control design, because both the optimal offsets between two crossover signals and the DDI's total system delay may vary with this critical variable. The cycle length constraints in this model were found to be critical to the resulting phasing plan and offsets as well as its performance. Hence, further research along this line will be devoted to the development of the design guide for setting the appropriate bounds for the DDI's cycle length under different design features and right-of-way constraints. In addition, coordinating the DDI's arterial through traffic flows with neighboring conventional intersections to prevent excessive queues on the connection bridge is also a critical issue and deserves further research. The coordination that considers other modes, such as pedestrians or cyclists, and their effects on the design of signal timings is another potential extension.

AUTHOR CONTRIBUTIONS

The authors confirm contribution to the paper as follows: study conception and design: Dawson Do, Yen-Yu Chen, Gang-Len Chang; data collection: Dawson Do, Yen-Yu Chen; analysis and interpretation of results: Yen-Yu Chen, Dawson Do; draft manuscript preparation: Dawson Do, Yen-Yu Chen, Gang-Len Chang. All authors reviewed the results and approved the final version of the manuscript.

REFERENCES

1. Nye, T. S., C. M. Cunningham, and E. Byrom. National-Level Safety Evaluation of Diverging Diamond Interchanges. *Transportation Research Record: Journal of the Transportation Research Board*, 2019. 2673:696-708.

2. Chlewicki, G. New Interchange and Intersection Designs: The Synchronized Split-Phasing Intersection and the Diverging Diamond Interchange. 2nd Urban Street Symposium: Uptown, Downtown, or Small Town: Designing Urban Streets That Work, Anaheim, CA, 2003.

3. Siromaskul, S., and S. B. Speth. A Comparative Analysis of Diverging Diamond Interchange Operations. ITE 2008 Annual Meeting and Exhibit, Institute of Transportation Engineers, Washington, DC, 2008.

4. Bared, J. G., P. K. Edara, and R. Jagannathan. Design and Operational Performance of Double Crossover Intersection and Diverging Diamond Interchange. *Transportation Research Record: Journal of the Transportation Research Board*, 2005. 1912:31-38.

5. Pang, B., H. Liu, and H. Xu. Calculating Approach Capacity of Diverging Diamond Interchanges with Consideration of Internal Queue Effects. *Transportation Research Record: Journal of the Transportation Research Board*, 2016. 2553:63-71.

6. Cohen, S. L., and C. C. Liu. The Bandwidth-Constrained TRANSYT Signal Optimization Program. *Transportation Research Record: Journal of the Transportation Research Board*, 1986. 1057:1-7.

7. Wong, C. K., and S. C. Wong. Lane-Based Optimization of Signal Timings for Isolated Junctions. *Transportation Research Part B: Methodological*, 2003. 37:63-84.

8. Gartner, N. H., J. D. Little, and H. Gabbay. Optimization of Traffic Signal Settings by Mixed-Integer Linear Programming: Part I: The Network Coordination Problem. *Transportation Science*, 1975. 9:321-343.

9. Little, J. D. C., M. D. Kelson, and N. H. Gartner. MAXBAND: A Program for Setting Signals on Arterials and Triangular Networks. *Transportation Research Record: Journal of the Transportation Research Board*, 1981. 795.

10. Day, C. M., Lavrenz, S. M., Stevens, A. L., Miller, R. E., and Bullock, D. M. Extending Link Pivot Offset Optimization to Arterials with Single Controller Diverging Diamond Interchange. *The 95th Transportation Research Board Annual Meeting*, Transportation Research Board of the National Academies, Washington, DC. 2016.

11. Day, C. M., and D. M. Bullock. Cycle-Length Strategies for a Diverging Diamond Interchange in a Coordinated Arterial. *Journal of Transportation Engineering*, 2016. 142:04016067.

12. Hainen, A. M., A. L. Stevens, C. M. Day, H. Li, J. Mackey, M. Luker, M. Taylor, J. R. Sturdevant, and D. M. Bullock. Performance Measures for Optimizing Diverging Diamond Interchanges and Outcome Assessment with Drone Video. *Transportation Research Record: Journal of the Transportation Research Board*, 2015. 2487:31–43.

13. Kim, S., S. Warchol, B. J. Schroeder, and C. Cunningham. Innovative Method for Remotely Fine-Tuning Offsets along a Diverging Diamond Interchange Corridor. *Transportation Research Record: Journal of the Transportation Research Board*, 2016. 2557:33-43.

14. Yang, X., G. L. Chang, and S. Rahwanji. Development of a Signal Optimization Model for Diverging Diamond Interchange. *Journal of Transportation Engineering*, 2014. 140:04014010.

15. Cheng, Y., G. L. Chang, and S. Rahwanji. Concurrent Optimization of Signal Progression and Crossover Spacing for Diverging Diamond Interchanges. *Journal of Transportation Engineering, Part A: Systems*, 2018. 144:04018001.

16. Coogan, S., and M. Thitsa. *Coordinated Anti-Congestion Control Algorithms for Diverging Diamond Interchanges*. No. FHWA-GA-21-1913. Georgia. Department of Transportation. Office of Performance-Based Management & Research, 2021.

17. Kukić, K. and A. Jovanović. Fuzzy Logic Approach on Traffic Control of a Diverging Diamond Interchange in Real Time. *ITM Web of Conferences*. Vol. 29. EDP Sciences, 2019.

18. Jovanović, A., K. Kukić, and A. Stevanović. A Fuzzy Logic Simulation Model For Controlling An Oversaturated Diverge Diamond Interchange And Ramp Metering System. *Mathematics and Computers in Simulation,* 2021. 182:165-181.

19. Yeom, C., B. J. Schroeder, C. Cunningham, K. Salamati, and N. M. Rouphail. Lane Utilization Model Development for Diverging Diamond Interchanges. *Transportation Research Record: Journal of the Transportation Research Board*, 2017. 2618:27-37.

20. Cunningham, C., Chase, T., Deng, Y., Carnes, C., Pyo, K., Jenior, P., Schroeder, B., Ray, B., Urbanik II, T., Knudsen, J., Rodegerdts, L., Warchol, S., Tanaka, A. *Diverging Diamond Interchange Informational Guide, Second Edition.* Washington, DC: The National Academies Press, 2021.

21. Cunningham, C., Schroeder, B. J., Phillips, S., Urbanik, T., Warchol, S., & Tanaka, A. Signal Timing for Diverging Diamond Interchanges: Fundamentals, Concepts, and Recommended Applications. *Transportation Research Record*, 2016. 2557:1-10.

22. Jenior, P., Haas, P. J., Butsick, A., & Ray, B. L. *Capacity Analysis for Planning of Junctions (CAP-X) Tool User Manual* (No. FHWA-SA-18-067). United States. Federal Highway Administration. Office of Safety, 2018.

23. PTV AG. *User's Manual, VISSIM 10*. Karlsruhe, Germany, 2018.

24. FICO. *Xpress-Optimizer Reference manual*, 33.01 edition, 2018.

25. McTrans, *TRANSYT-7F Users Guide*. University of Florida, Florida, 2009.